Arch. Min. Sci. **64** (2019), 1, 181-196

Electronic version (in color) of this paper is available: http://mining.archives.pl

DOI 10.24425/ams.2019.126279

NAN YAO*, YI-CHENG YE*,**, BIN HU*, WEI-QI WANG*, QI-HU WANG*#

PARTICLE FLOW CODE MODELING OF THE MECHANICAL BEHAVIOR OF LAYERED ROCK UNDER UNIAXIAL COMPRESSION

MODELOWANIE WŁAŚCIWOŚCI MECHANICZNYCH SKAŁ WARSTWOWYCH W WARUNKACH ŚCISKANIA JEDNOOSIOWEGO PRZY ZASTOSOWANIU OPROGRAMOWANIA PARTICLE FLOW CODE (PFC)

In this paper, the different mechanical behaviors of layered rocks with different bedding angles during uniaxial compression tests are studied. Numerical simulation models of layered rock are validated based on laboratory tests, and uniaxial compression tests are conducted by using *Particle Flow Code* (PFC). Using these simulations, the uniaxial compressive strength, failure patterns, development of micro-cracks, and displacement of meso particles are analyzed. When the bedding angle is similar to the failure angle, the macro failure planes develop directly along the beddings, the bedding behavior dictates the behavior of the layered rock, reducing the compressive strength.

Keywords: Layered rock; Uniaxial compression test; Particle Flow Code (PFC); Bedding angle; Micro--cracks

W pracy badano właściwości mechaniczne skał warstwowych zalegających pod różnym kątem uwarstwienia w warunkach ściskania jednoosiowego. Walidację modeli symulacyjnych skał warstwowych przeprowadzono w oparciu o wyniki badań laboratoryjnych, zaś testy ściskania jednoosiowego prowadzono z użyciem pakietu *Particle Flow Code* (PFC). W oparciu o badania symulacyjne, analizowano wytrzymałość skał na ściskanie jednoosiowe, modele pękania, powstawanie mikropęknięć i przemieszczenia mezo- cząstek. W przypadku gdy kąt płaszczyzny uwarstwienia ma wartość przybliżoną do kąta pęknięcia, płaszczyzny pękania w skali makro pojawiają się wzdłuż spękań, a układ warstw skalnych determinuje ich wytrzymałość na ściskanie, powodując jej obniżenie.

Słowa kluczowe: skała warstwowa, wytrzymałość ściskanie jednoosiowe, Particle Flow Code (PFC), kąt uwarstwienia, mikropęknięcia

* SCHOOL OF RESOURCES AND ENVIRONMENTAL ENGINEERING, WUHAN UNIVERSITY OF SCIENCE AND TECHNOLOGY, WUHAN 430081, CHINA

** HUBEI KEY LABORATORY FOR EFFICIENT UTILIZATION AND AGGLOMERATION OF MET ALLERGIC MINERAL RESOURCE, WUHAN 430081, CHINA

\# Corresponding author: wangqihu@wust.edu.cn

1. Introduction

Layered rock is one of the most common rock types on the earth's surface, it is widely encountered in all kinds of geotechnical engineering (Saroglou, 2013; Chang et al., 2016; Xu et al., 2017). The heterogeneity of layered rock is widely varied (Tien & Kuo, 2001; Shi et al., 2016), and many scholars have studied the physical and mechanical characteristics of layered rock through laboratory rock mechanics tests, similar physical tests of fabricated samples, and numerical simulations (Tien & Tsao, 2000; Yasar, 2001; Lin et al., 2013). Although Liao et al. (1997) and Tan et al. (2015), researched the direct tensile behavior and Brazilian test behavior of layered rock, respectively, most researchers have focused on the variations of compressive strength with different bedding angles.

In this realm of study, Niandou et al. (1997), Nasseri et al. (2003), Fahimifar (2004), and Zhang et al. (2010) studied the influence of different bedding angles on the compressive strength of layered rocks through uniaxial compression tests and triaxial compression tests of Tournemire shale, Himalayan schists, Isfahan schists, and sandstone specimens, respectively. Owing to the difficulty of sampling layered rock specimens, some scholars have used similar materials to emulate layered rock and performed corresponding research with artificial layered rock. For example, Tien et al. (2006) studied the failure mechanism of artificial transversely isotropic rocks, and Sahouryeh et al. (2002), Dyskin et al. (2003) and Park and Bobet (2010) fabricated layered rock with similar rock material, like gypsum or resin, and studied its mechanical behavior. On the study of the strength criterion of layered rock, Saroglou and Tsiambaos (2008), Saeidi et al. (2014), and Ismael et al. (2014) defined a modified Hoek-Brown strength criterion to predict the strength of layered rock with different bedding angles based on numerous test data for layered rock under uniaxial and triaxial compression. Singh and Singh (2012) and Singh et al. (2015) defined modified Mohr-Coulomb strength criterions for layered rock and validated the criterion through many test data. Shi et al. (2016) studied the variations of friction angles and the cohesions of the layered rock with different bedding angles.

Few articles showed the failure characteristics of layered rock, namely, research on the mechanical behavior of layered rock with different bedding angles is very rare, especially the generating mechanism for the different failure characteristics between layered rocks with different bedding angles. In this study, numerical models of layered rock are generated, and uniaxial compression tests are simulated using Particle Flow Code (PFC) to research how different bedding angles influence the mechanical behavior of layered rocks under uniaxial compression. These simulations are validated by experimental results. Based on the numerical simulation test results and analysis of the development law for micro-cracks and the displacement of meso particles in different numerical specimens with different bedding angles, the uniaxial compression failure patterns of layered rock with different bedding angles are analyzed at the meso-level, and their mechanical failure mechanisms under uniaxial compression are also revealed.

2. Methods

2.1. Original Layered Rock Samples

The recommendations of Bieniawski and Bernede (1979) were followed strictly during sample preparation and testing. Cylindrical specimens, with a diameter of 50 mm and a height

of 100 mm, were acquired, and the errors were controlled within 2%. First, cylindrical cores with a diameter of 50 mm were drilled out from siliceous shale rock blocks. The siliceous shale rock blocks were sampled from Zhanghai Gold Mine in Daye City, Hubei Province, China. Then, the cores were cut into test specimens of suitable length. It was especially ensured that the axis of the specimens was perpendicular to both of the end faces, which were ground for flatness (Tan et al., 2015). The acquired specimens of layered rock, with bedding angles of 0°, 15°, 30°, 45°, and 60°, are shown in Fig. 1; however, those with bedding angles of 75° or 90° were not drilled out successfully. A uniaxial rock test system was used for the uniaxial compression tests.

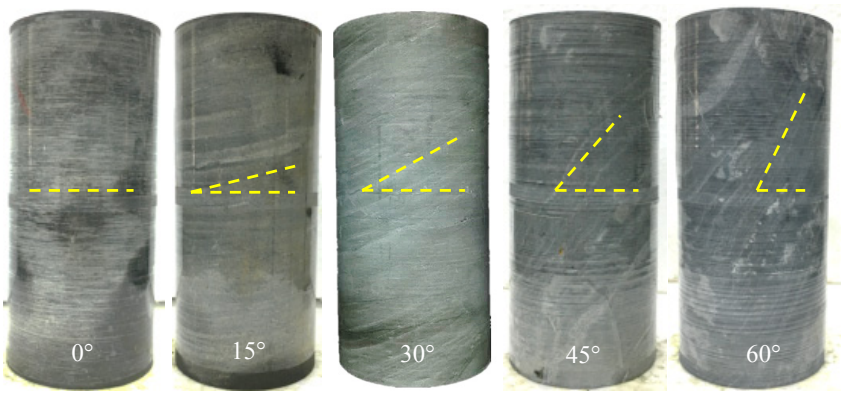

Fig. 1. Specimens of layered rock

2.2. Numerical Layered Rock Models

2.2.1. Meso-parameters of PFC model

In the PFC 2D model, particles are discrete disks with infinite stiffness, parallel bond model can not only transmit force but also torque, so it is more suitable for mechanical analysis of rock materials. The particles are connected by the parallel bond in the PFC system, resulting in a continuous and complete rock model. In the model, the particle motion obeys Newton's second law, and the interactions between particles obey the force-displacement law. The failure of rock is the breaking of bonds at the meso-level. Normal stress σ and tangential stress τ acting on parallel bond can be calculated according to formula (1) and (2).

$$\sigma_{\max} = \frac{-\bar{F}_i^n}{A} + \frac{\left|\bar{M}_i^s\right|}{I}\bar{R} \tag{1}$$

$$\tau_{\max} = \frac{\left|\bar{F}_i^s\right|}{A} + \frac{\left|\bar{M}_i^n\right|}{J}\bar{R} \tag{2}$$

In these formulas, $\bar{R}$ is the radius of parallel bond; $\bar{F}_i^n$, $\bar{F}_i^s$, $\bar{M}_i^n$ and $\bar{M}_i^s$ are the normal strength, shear strength, normal bending moment and shear bending moment of parallel bond,

respectively; I, J and A are the moment of inertia, polar moment of inertia and cross-sectional area of parallel bond, respectively.

There are mainly three types of meso-parameters for a PFC model of layered rock: particle attribute parameters, particle-bonded attribute parameters, and bedding attribute parameters (Li & Holt, 2002; Cho et al., 2007). In particular, the bedding attribute parameter only includes one parameter, i.e., the weakening factor for particle and particle-bonded attribute parameters. The parallel bond model was selected as the bond form of particles (Jin et al., 2017). According to the laboratory test results, the density of siliceous shale is 2565 kg/m^3, its uniaxial compressive strength when the bedding is horizontal ($\beta = 0°$) is 84.11 MPa, and its elastic modulus and Poisson's ratio are 14.23 GPa and 0.22, respectively. To match the properties of siliceous shale, the final meso-parameters of the PFC model after repeated testing can be seen in Table 1.

TABLE 1

Meso-parameters for parallel bond particle model

Types of meso-parameters	Parameters		Values
Particle	E_c	Young's modulus [GPa]	8
	k_n/k_s	Stiffness ratio	2
	μ	Friction coefficient	0.6
	R_{max}/R_{min}	Radius ratio	1.66
	R_{min}	Minimum radius [mm]	0.25
	ρ	Density [kg/m^3]	2565
Particle-bonded	$\bar{E}_c$	Young's modulus [GPa]	8
	$\bar{k}_n/\bar{k}_s$	Stiffness ratio	2
	$\bar{\sigma}_c$	Normal strength [MPa]	30±6
	$\bar{\tau}_c$	Shear strength [MPa]	60±12
	λ	Radius multiplier	1.5
Bedding	η	Weakening factor	0.25

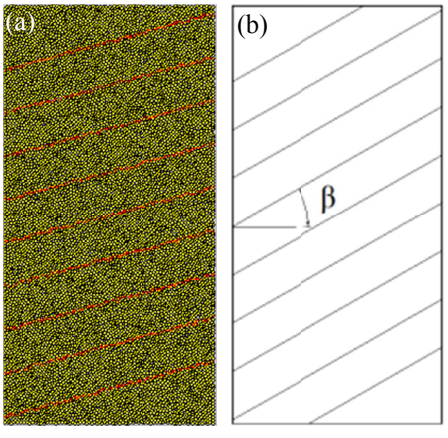

Fig. 2. Numerical specimens of layered rock: (a) Particle model; (b) Bedding model

2.2.2. Numerical specimens of layered rock

The numerical specimens of layered rock were generated with the built-in Fish function of PFC after inputting the meso-parameters from Table 1. The 2D model, with dimensions of 100 mm (height) × 50 mm (diameter), is shown in Fig. 2. Seven models were generated with different bedding angles (β = 0°, 15°, 30°, 45°, 60°, 75°, and 90°). In order to prevent different bedding densities from impacting the strengths of the layered rocks with different bedding angles, the vertical distance between boundaries of neighboring beddings was set at 10 mm in

every numerical specimen. There are 12092 particles in each model. The upper and lower end faces of the model are constrained by rigid walls, which were slowly moved to simulate the uniaxial compression test.

3. Results

3.1. Validation results from uniaxial compression tests

Fig. 3 shows a comparison of stress-strain curves of the original and numerical layered rocks when the bedding angle is 0°. Fig. 4 shows comparisons of failure patterns of the original and numerical layered rocks with different bedding angles. These results show that the macro mechanical behavior of numerical layered rock, such as stress-strain curves and failure patterns, and other mechanical parameters, like uniaxial compressive strength, elastic modulus, and Poisson's ratio, are basically consistent with the original layered rock, which shows that the meso-parameters of numerical layered rock are adequate for simulation of the original layered rock.

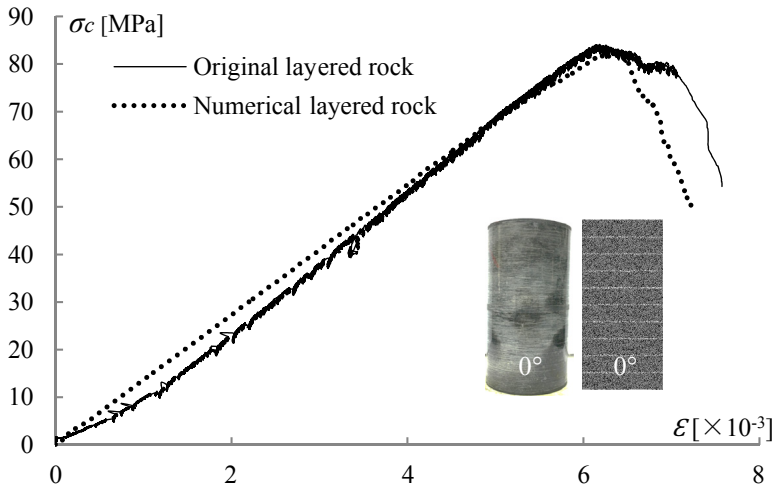

Fig. 3. Stress-strain curves of layered rocks with a bedding angle of 0°

The uniaxial compressive stress-strain curves for numerical layered rocks with different bedding angles are shown in Fig. 5; the uniaxial compressive strength of layered rocks from laboratory tests and numerical simulations are shown in Fig. 6. Fig. 5 and Fig. 6 show that the uniaxial compressive strength of layered rocks initially decreases and then increases with the increase bedding angles. The strengths are categorically higher when β = 0°, 15°, 30°, 45°, or 90° than when β = 60° or 75°; the strength reduction of the numerical specimens when β = 60° and 75° is quite significant. The strength is fairly constant for β ranging between 0° and 45°. The asymmetrical uniaxial compressive strength curve of layered rocks with different bedding angles complies with the weak surface fracture criterion (Jaeger and Cook 1976; Saroglou and

Tsiambaos 2008). The influence of the bedding angle on the uniaxial compressive strength of layered rocks is small when $\beta < 45°$ and $\beta = 90°$; however, the influence is big when β ranges from 45° to 90°.

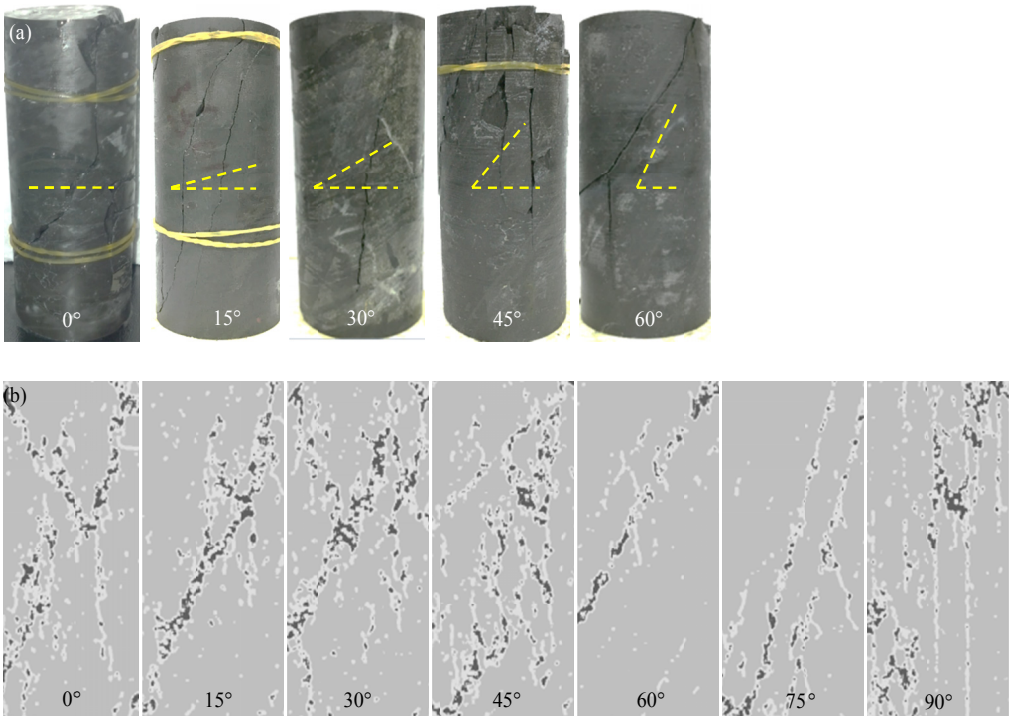

Fig. 4. Failure specimens of layered rock: (a) Laboratory test; (b) Numerical test

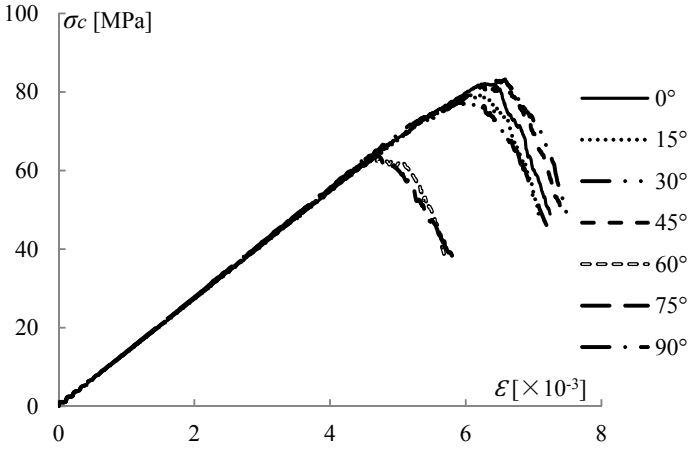

Fig. 5. Stress-strain curves of numerical specimens

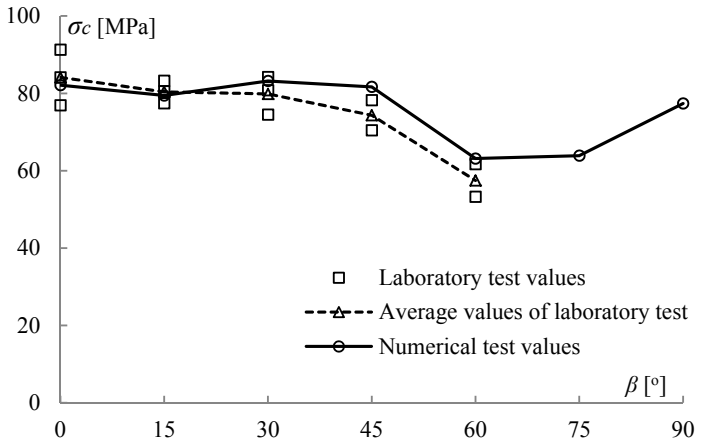

Fig. 6. Uniaxial compressive strength of layered rocks with different bedding angles

3.2. Failure Patterns of Layered Rock

The failure patterns of layered rocks with different bedding angles – as shown in Fig. 4 – can be summarized as follows:

(1) Conical failure planes are formed in one side of the specimens and tensile failure planes develop beneath the cone top when $\beta = 0°$.
(2) The macro failure planes of the specimens are smooth slopes that penetrate through multiple beddings when $\beta = 15°$ and 30°.
(3) The macro failure planes of the specimens are complicated when $\beta = 45°$; there are both failure planes along the beddings and through beddings; the failure patterns of the specimens are the transitional pattern of $\beta = 15°$ or 30° and $\beta = 60°$ or 75°.
(4) The macro failure planes develop directly along the beddings when $\beta = 60°$ and 75°; the failure patterns are mainly led by the weak surface.
(5) There are numerous failure planes along the vertical beddings and several failure planes across the intact rocks between the vertical beddings when $\beta = 90°$; the failure patterns are mainly splitting failure.

Although the specimens could not be prepared in the laboratory test with $\beta = 75°$ or 90° for comparison with the corresponding numerical simulation results, the failure patterns of the numerical specimens with different bedding angles are generally consistent with the test results of Yasar (2001), Tien et al. (2006) and Zhang et al. (2010).

The above failure patterns and uniaxial compressive strength of layered rocks with different bedding angles appear to exhibit some similar tendencies. The influence of bedding angle on both the failure patterns and uniaxial compressive strength of layered rock are small when $\beta < 45°$ (especially gently inclined layered rock); likewise, the failure patterns and strength are mainly determined by the strength of intact rocks between beddings. For example, the layered rock is transversely isotropic rock when $\beta = 0°$, in which case the failure planes are symmetrical tensile failure planes. In contrast, the failure planes develop directly along the beddings when $\beta = 60°$ and 75°, so the uniaxial compressive strength is instead determined by the strength

of weak surface (i.e., bedding). Exceptionally, the failure planes are both along beddings and in the intact rocks between beddings when $\beta = 90°$; the strength of rock is greater than that of beddings, so the uniaxial compressive strength is determined by the strength of intact rocks between beddings.

According to Coulomb's "friction criteria" (Brady & Brown, 1994), the failure angle, θ, between the normal direction of the main failure plane and the direction of the maximum principal stress – as shown in Fig. 7 – is

$$\theta = \frac{\pi}{4} + \frac{\varphi}{2} \tag{3}$$

where φ is the internal friction angle of the rock, whose value is between 30° and 60° for common rocks. Thus, so the value of θ ranges from 60° to 75° correspondingly.

The failure angles of most specimens ranged from 60° to 75°, except $\beta = 0°$ and 90° (see Fig. 4), which is in accordance with Coulomb's "friction criteria". The failure planes will develop directly along the beddings if $\beta \approx \theta$ (i.e., when $\beta = 60°$ or 75°); however, the failure planes will slope through multiple beddings if the bedding angles of layered rock are far smaller than θ (i.e., gently inclined layered rock).

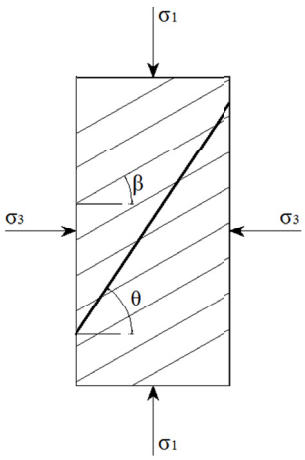

Fig. 7. Failure angle, θ, in layered rock

3.3. Micro-crack Development of Layered Rock

The relations between micro-crack development and vertical displacement in layered rocks with different bedding angles are shown in Fig. 8. The total number of micro-cracks in every specimen increases nonlinearly with the increase of vertical displacement, i.e., the early growth is slow, the later growth is faster, and micro-cracks develop most rapidly in the stage after peak strength. Micro-cracks begin developing at a smaller vertical displacement in the specimens when $\beta = 60°$ and 75° than in the other specimens, and the total number of micro-cracks is approximately one third of that for other specimens. This occurs because the beddings are weak, and the failure planes develop directly along the beddings, so micro-cracks develop less frequently in the intact rock between beddings. As with the uniaxial compressive strength and failure patterns of the specimens when $\beta = 60°$ and 75°, the development patterns of micro-cracks behave differently than in the other specimens.

4. Discussion

Fig. 4 and Fig. 6 show that the layered rocks with different bedding angles differ not only different in strength, but also in their failure patterns. According to the above analysis of uniaxial compressive strength, failure patterns, and micro-crack development characteristics of layered

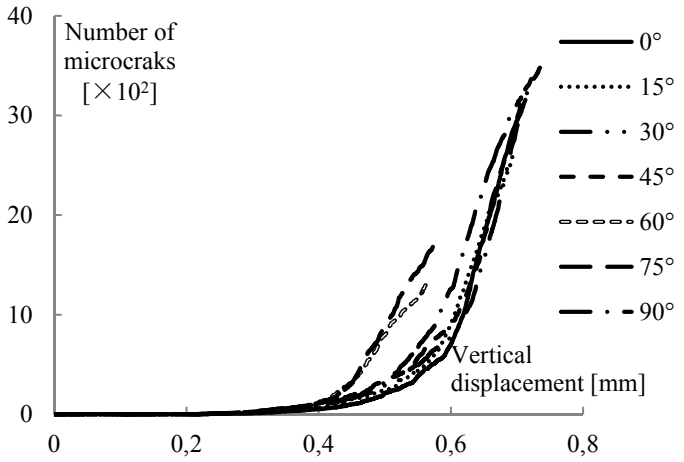

Fig. 8. Relations between micro-crack development and vertical displacement

rocks with different bedding angles, four typical layered rocks with different bedding angles ($\beta = 0°$, 30°, 60°, and 90°) were selected as research samples. Using these samples, the uniaxial compression mechanical behavior of layered rock is analyzed based on the meso-mechanical response during uniaxial compression; the strength and number of micro-cracks are shown in Fig. 9. Eight monitoring points with different steps are set during the uniaxial compression of each specimen (See Fig. 9) – the setting instructions for the monitoring points are shown in Table 2.

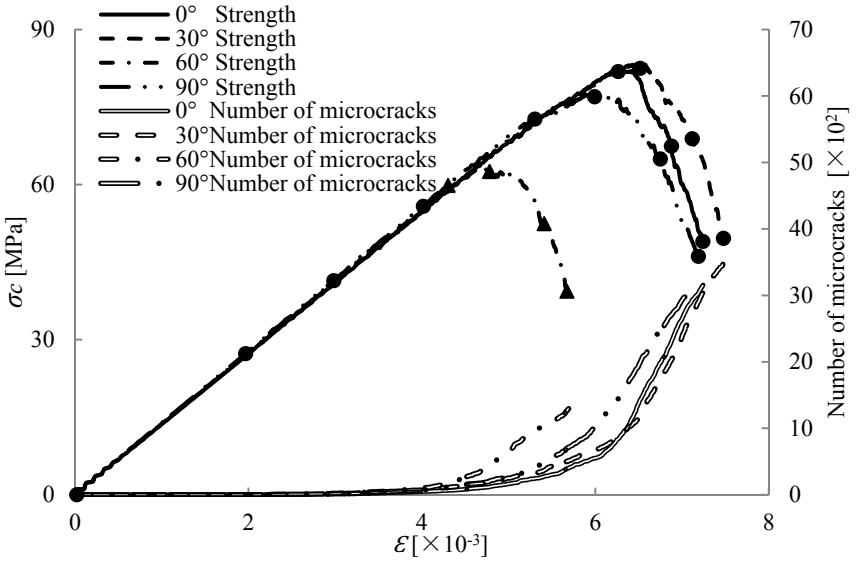

Fig. 9. Uniaxial compression test results for four layered rocks with different bedding angles (monitoring points denoted on strength curves)

TABLE 2

Settings for monitoring points

Monitoring points	Stage of test	ε [$\times 10^{-3}$]	Remarks
i	Starting point	0	Same for all four specimens
ii	Line elastic point	2	
iii	Line elastic point	3	
iv	Line elastic point	4	
v	Yield point	—	Same for 3 specimens (not 60°)
vi	Peak point	—	Different for all 4 specimens
vii	Mid-point between peak and end	—	
viii	End point	—	

4.1. Development of Micro-crack Distributions

According to the theories of damage mechanics and fracture mechanics, when rock material is subjected to external load, its meso-structure will exhibit either meso-damage or micro-cracks. In the PFC model, the microscopic embodiment is that the tensile or shear load acting on the bond structure exceeds the tensile or shear strength of the bonds between the particles in the structure, resulting in the bonds breaking and corresponding tensile or shear cracks. With the sustained effect of the load, the micro-cracks develop further, expanding and connecting, eventually leading to macro failure of the rock material.

The micro-crack distributions in the four specimens are presented in Fig. 10 for all but the first two monitoring points because no micro-cracks form in these steps. In Fig. 10, the tensile cracks are blue and the shear cracks are red. The tensile cracks are much more numerous than shear cracks in the numerical specimens, most of the shear cracks are distributed in the concentrated areas of tensile cracks, indicating that the concentrated areas of tensile failure are often accompanied by shear failure.

The initial micro-cracks were evenly distributed in the specimen when $\beta = 0°$ (see *iii*, *iv*, and *v* in Fig. 10(a)). With the continued loading, the compressive stress is gradually converted into tensile stress owing to the high compressive and low tensile properties of the rock material, resulting in the gradual connection of the tensile cracks to form several sets of small, parallel, and diagonal cracks (see *vi* in Fig. 10(a)). The small cracks gradually converge, and further development and expansion causes the final macro failure planes (see *vii* and *viii* in Fig. 10(a)). In addition, because the small cracks converge simultaneously, the shear cracks also show a degree of development in the concentrated areas of tensile cracks.

The initial micro-cracks were also evenly distributed in the specimen when $\beta = 30°$ (see *iii*, *iv*, and *v* in Fig. 10(b)). The distribution of small cracks is less structured compared to those in the specimen with $\beta = 0°$ (compare to *vi* in Fig. 10(a)), and the micro-cracks converge along the final failure planes earlier than in the specimen with $\beta = 0°$ (see *vi*, *vii*, and *viii* in Fig. 10(b)). Shear cracks develop in both the final failure planes and the beddings.

The initial micro-cracks are distributed in the beddings when $\beta = 60°$, and a concentration of such cracks appears in one of the beddings (see *v* and *vi* in Fig. 10(c)). Subsequently, micro-cracks (including tensile and shear cracks) rapidly develop in this bedding – developing slowly in the other beddings – and the final failure planes form along the bedding (see *vii* and *viii* in Fig. 10(c)).

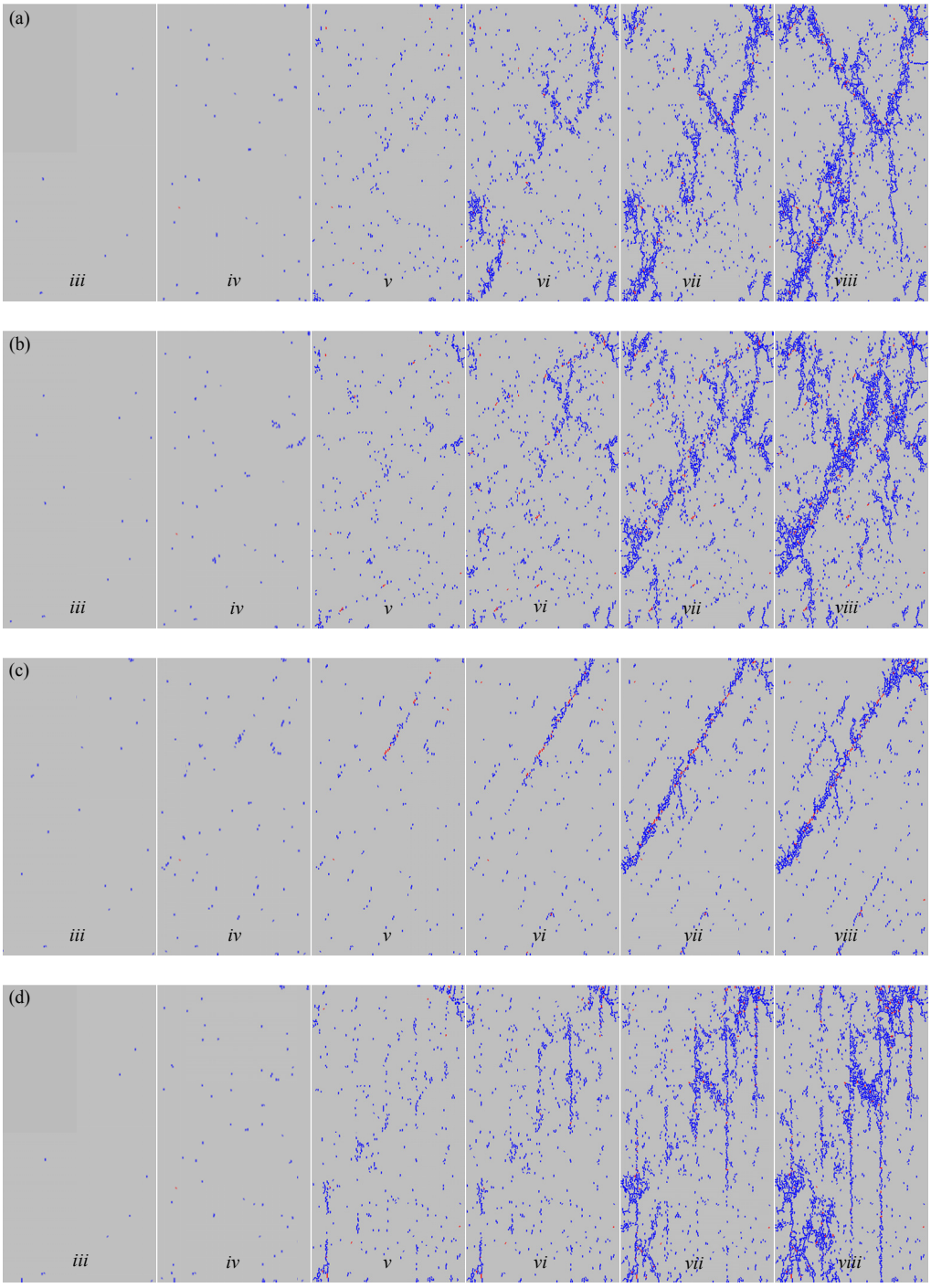

Fig. 10. Micro-cracks distributions at different steps: (a) $\beta = 0°$; (b) $\beta = 30°$; (c) $\beta = 60°$; (d) $\beta = 90°$

When $\beta = 90°$, the micro-cracks develop in both the vertical beddings and the intact rocks between them, but more in beddings than in the rocks because that the beddings are weaker than the intact rocks (see *v* and *vi* in Fig. 10(d)). The final splitting failure planes finally form along the vertical beddings and tensile failure planes in the intact rocks between beddings with the continuous development of micro-cracks in these areas (see *vii* and *viii* in Fig. 10(d)). The complex failure planes in the specimen show that the splitting failures along the beddings do not completely damage the specimen because the intact rocks between the vertical beddings still have strength; only the failure of the intact rocks can lead to the final failure of the specimen.

4.2. Displacement of Meso Particles

Fig. 11 shows three types of local particle displacement fields. According to Zhang and Wong's research (2014), DF_I is relative tensile displacement, presented as two vectors diverging from each other; DF_II exhibits both relative tensile and shear displacement, and DF_III exhibits relative shear displacement, presented as two vectors converging from two opposite directions.

The displacement of meso particles in the typical monitoring area of four specimens at three steps are presented in Fig. 12. Fig. 13 shows the monitoring area of specimen.

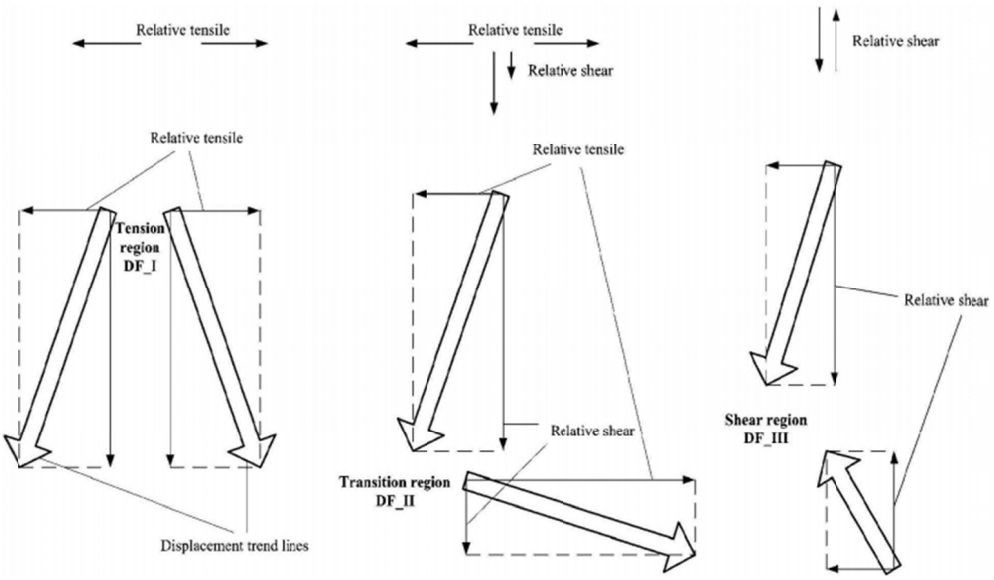

Fig. 11. Three displacement field types defined by displacement trend lines (Zhang & Wong, 2014)

From Fig. 9, Point *ii* is the Line elastic point, the displacement direction of meso particles in the top part of specimen is mainly downwards, and which of those in the bottom part is opposite (see *ii* in Fig. 12(a), (b), (c) and (d)), there are no obvious differences in the specimens with different bedding angles. Furthermore, the meso particles in both left and right part also have outwards displacement, the more the particles near the left or right boundaries and the middle, the more obvious the phenomenon is. The above two kinds of phenomena meet the behavior of

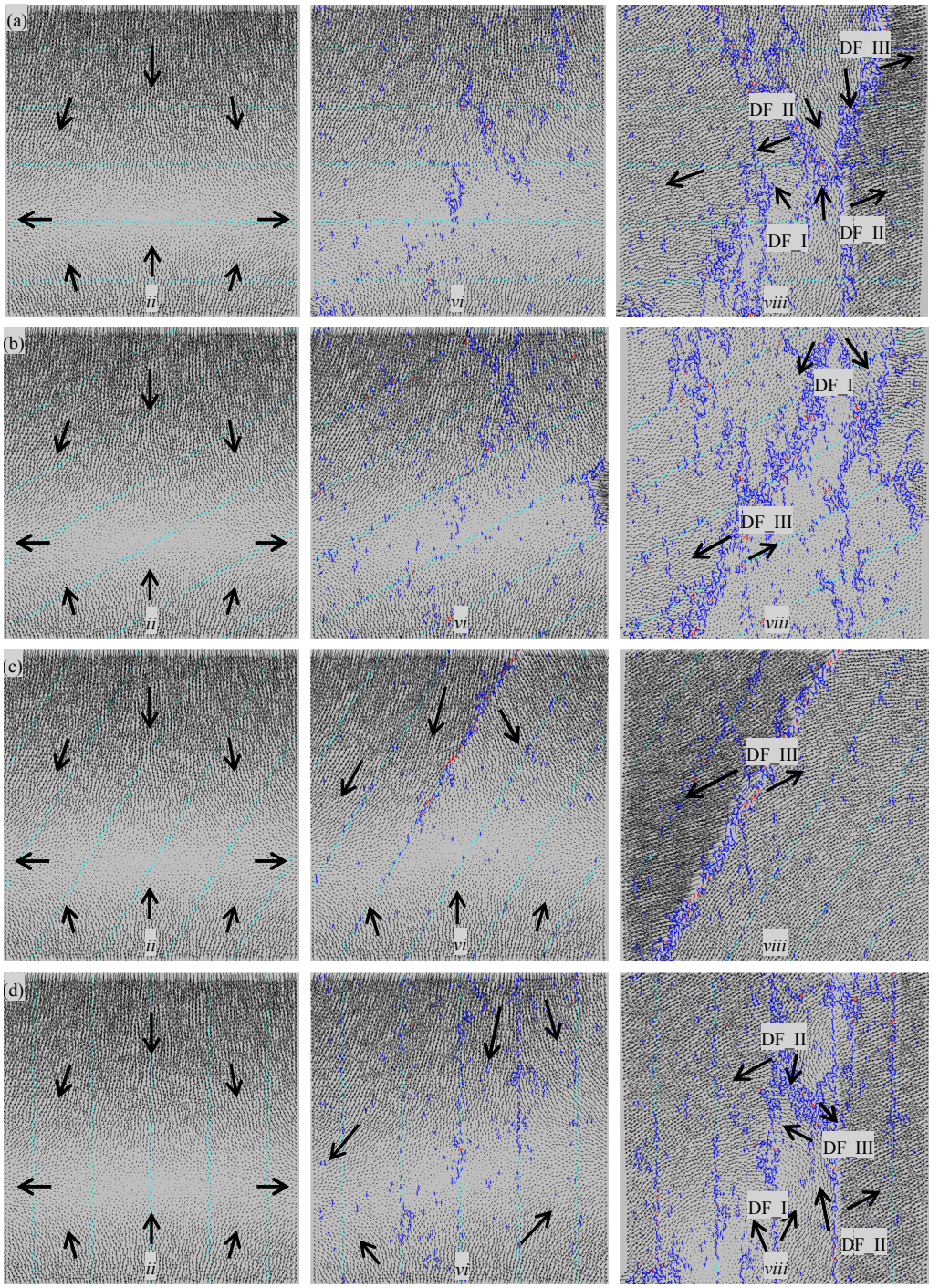

Fig. 12. Displacement of meso particles: (a) $\beta = 0°$; (b) $\beta = 30°$; (c) $\beta = 60°$; (d) $\beta = 90°$

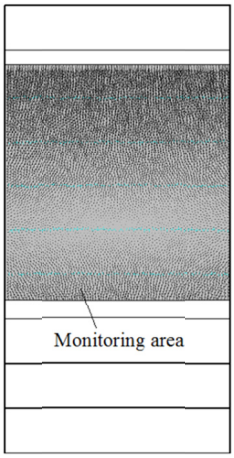

Fig. 13. The monitoring area of specimen

"rock compaction" and "rock expansion" respectively in the line elastic phase of compression test.

Point *vi* is the Peak point, the displacement of meso particles at this point seem the same with which at Point *ii* when $\beta = 0°$ and 30° (see *vi* in Fig. 12(a) and (b)), but the displacement directions of meso particles have significant changes near some beddings when $\beta = 60°$ and 90°, i.e., meso particles at two sides of some beddings are separated (see *vi* in Fig. 12(c) and (d)). The differences of displacement vectors at Point *vi* between $\beta = 0°$ or 30° and $\beta = 60°$ or 90° also show that the bedding orientation has significant influence of the displacement of meso particles and the failure patterns when $\beta > 45°$, and the influence is smaller when $\beta < 45°$. The development of meso particles' displacement and macro failure planes are earlier when $\beta > 45°$ than $\beta < 45°$.

Point *viii* is the End point of compression test. The displacement vectors of layered rocks with four kinds of different bedding angles (see *viii* in Fig. 12(a), (b), (c) and (d)) can be summarized as follows:

(1) The displacement vectors present DF_II and DF_III near the conical failure planes, and DF_I and DF_II beneath the cone top when $\beta = 0°$, which mean that tensile-shear combined and shear failure develop near the conical failure planes, and tensile and tensile-shear combined failure develop beneath the cone top.
(2) The mainly type of displacement field is DF_III, and DF_I is presented in few areas when $\beta = 30°$, which mean that mainly shear failure and little tensile failure develop in the specimen in the situation of single slope failure pattern.
(3) The displacement vectors are only distributed as DF_III when $\beta = 60°$, which mean that shear failure in the specimen in the situation of failure planes along the bedding.
(4) The displacement vectors present DF_I and DF_II near the vertical beddings, and DF_ III near the failure planes in the intact rock between two vertical beddings when $\beta = 90°$, which mean that tensile and tensile-shear combined failure develop near the vertical beddings, and shear failure develop in the intact rock between two vertical beddings.

4.3. Relations between micro-crack and failure and strength

The above analysis of micro-crack development processes and displacement of meso particles further illustrates that the influences of beddings on both the failure patterns and uniaxial compressive strength of layered rock are obvious. The influence features can be summarized as follows:

(1) When $\beta = 0°$ or 30°, tensile-shear combined and shear failure develop in the intact rocks between beddings, which cause the macro failure planes penetrate through multiple beddings, the failure is mainly determined by the mechanical properties of the intact rocks between beddings. Furthermore, the failure patterns are the embodiment of the effect of "pressure-induced pull" in the uniaxial compression process.
(2) when $\beta = 60°$, shear failure develops along the bedding, which cause the failure planes develop directly along the beddings, the strength is mainly determined by the mechanical properties of the beddings. Therefore, the influence of beddings on both the failure pat-

terns and uniaxial compressive strength of layered rock is significant, and the influence of the mechanical properties of the intact rocks between the beddings is limited.

(3) when $\beta = 90°$, tensile and tensile-shear combined failure develop near the vertical beddings, and shear failure develop in the intact rock between two vertical beddings, which cause the failure planes of the specimen are along the vertical beddings and across the intact rocks between vertical beddings. Although the failure patterns are mainly affected by the bedding orientation, the strength is mainly determined by the mechanical properties of the intact rocks between beddings.

5. Conclusions

Based on the laboratory test results of siliceous shale under uniaxial compression, numerical simulation models of layered rock were validated, and uniaxial compression tests were conducted using PFC. The uniaxial compressive strength and failure patterns of the numerical specimens had good consistency with the laboratory test results, which showed that the meso-parameters of numerical layered rock are adequate for simulation of the original layered rock. The analysis of the uniaxial compressive strength, failure patterns, development processes of micro-cracks, and displacement of meso particles of layered rocks with different bedding angles from numerical simulations showed that the trends of these characteristics are consistent with each other. Furthermore, the mechanical behavior of layered rock under uniaxial compression was revealed by combining the four aspects of analysis.

The bedding angle had important influence on the mechanical behavior of the layered rock under uniaxial compression. The uniaxial compressive strength of the layered rocks initially decreases and then increases as the bedding angle increases. Additionally, the strengths were categorically higher when $\beta = 0°$, 15°, 30°, 45°, or 90° than when $\beta = 60°$ and 75°. Likewise, the failure behavior and development of micro-cracks differed between these two categories. When the bedding angle is similar to the failure angle (i.e., β between 60° and 75°), failure occurs in the bedding along the layer angle with fewer micro-cracks than in other cases.

Acknowledgements

This work was supported by the National Natural Science Foundation of China [grant number 51574183]. We would like to thank Editage [www.editage.cn] for English language editing.

References

Bieniawski Z.T., Bernede M.J., 1979. *Suggested methods for determining the uniaxial compressive strength and deformability of rock materials: Part 1. Suggested method for determining deformability of rock materials in uniaxial compression*. International Journal of Rock Mechanics & Mining Sciences & Geomechanics Abstracts **16** (2), 138-140.

Brady B.H.G., Brown E.T., 1994. *Rock mechanics for underground mining*. Chapman & Hall, London.

Chang X., Wang J.H., Tang C.A., Ru Z.L., 2016. *Effects of interface behavior on fracture spacing in layered rock*. Rock Mechanics & Rock Engineering **49** (5), 1733-1746.

Cho N., Martin C.D., Sego D.C., 2007. *A clumped particle model for rock*. International Journal of Rock Mechanics & Mining Sciences **44** (7), 997-1010.

Dyskin A.V., Sahouryeh E., Jewell R.J., Joer H., Ustinov K.B., 2003. *Influence of shape and locations of initial 3-D cracks on their growth in uniaxial compression*. Engineering Fracture Mechanics **70** (15), 2115-2136.

Fahimifar A., 2004. *Strength and deformation properties of a schist rock in Isfahan*. Iranian Journal of Science & Technology, Transaction B **28** (B5), 619-622.

Ismael M.A., Imam H.F., EI-Shayeb Y., 2014. *A simplified approach to directly consider intact rock anisotropy in Hoek-Brown failure criterion*. Journal of Rock Mechanics and Geotechnical Engineering **6** (5), 486-492.

Jaeger J.C., Cook N.G.W., 1976. *Fundamentals of rock mechanics*. Chapman & Hall, London.

Jin J., Cao P., Chen Y., Pu C.Z, Mao D.W., Fan X., 2017. *Influence of single flaw on the failure process and energy mechanics of rock-like material*. Computers & Geotechnics **86**, 150-162.

Li L., Holt R.M., 2002. *Particle scale reservoir mechanics*. Oil & Gas Science and Technology **57** (5), 525-538.

Liao J.J., Yang M.T., Hsieh H.Y., 1997. *Direct tensile behavior of a transversely isotropic rock*. International Journal of Rock Mechanics & Mining Sciences **34** (5), 837-849.

Lin H., Cao P.,Wang Y.X., 2013. *Numerical simulation of a layered rock under triaxial compression*. International Journal of Rock Mechanics & Mining Sciences **60** (6), 12-18.

Nasseri M.H.B, Rao K.S., Ramamurthy T., 2003. *Anisotropic strength and deformational behavior of Himalayan schists*. International Journal of Rock Mechanics & Mining Sciences **40** (1), 3-23.

Niandou H., Shao J.F., Henry J.P., Fourmaintraux D., 1997. *Laboratory investigation of the mechanical behaviour of Tournemire shale*. International Journal of Rock Mechanics & Mining Sciences **34** (1), 3-16.

Park C.H., Bobet A., 2010. *Crack initiation, propagation and coalescence from frictional flaws in uniaxial compression*. Engineering Fracture Mechanics **77** (14), 2727-2748.

Saeidi O., Rasouli V., Vaneghi R G, Gholami R., Torabi S.R., 2014. *A modified failure criterion for transversely isotropic rocks*. Geoscience Frontiers **5** (2), 215-225.

Sahouryeh E., Dyskin A.V., Germanovich L.N., 2002. *Crack growth under biaxial compression*. Engineering Fracture Mechanics **69** (18), 2187-2198.

Saroglou H., 2013. *Engineering behaviour of anisotropic and heterogeneous layered rocks*. Proc. of Iaeg Conf. Global View of Engineering Geology and the Environment, 721-731.

Saroglou H., Tsiambaos G., 2008. *A modified Hoek-Brown failure criterion for anisotropic intact rock*. International Journal of Rock Mechanics & Mining Sciences **45** (2), 223-234.

Shi X.C., Yang X., Meng Y.F., Gao L., 2016. *An anisotropic strength model for layered rocks considering planes of weakness*. Rock Mechanics & Rock Engineering **49** (9), 1-10.

Singh M., Samadhiya N.K., Kumar A., Kumar V., Singh B., 2015. *A nonlinear criterion for triaxial strength of inherently anisotropic rocks*. Rock Mechanics & Rock Engineering **48** (4), 1387-1405.

Singh M., Singh B., 2012. *Modified Mohr-Coulomb criterion for non-linear triaxial and polyaxial strength of jointed rocks*. International Journal of Rock Mechanics & Mining Sciences **51** (2), 43-52.

Tan X., Konietzky H., Frühwirt T., Dan D.Q. 2015. *Brazilian tests on transversely isotropic rocks: laboratory testing and numerical simulations*. Rock Mechanics & Rock Engineering **48** (4), 1341-1351.

Tien Y.M., Kuo M.C., 2001. *A failure criterion for transversely isotropic rocks*. International Journal of Rock Mechanics & Mining Sciences **38** (3), 399-412.

Tien Y.M., Kuo M.C., Juang C.H., 2006. *An experimental investigation of the failure mechanism of simulated transversely isotropic rocks*. International Journal of Rock Mechanics & Mining Sciences **43** (8), 1163-1181.

Tien Y.M., Tsao P.F., 2000. *Preparation and mechanical properties of artificial transversely isotropic rock*. International Journal of Rock Mechanics & Mining Sciences **37** (6), 1001-1012.

Xu D.P., Feng X.T., Chen D.F., Zhang C.Q., Fan Q.X., 2017. *Constitutive representation and damage degree index for the layered rock mass excavation response in underground openings*. Tunnelling & Underground Space Technology **64**, 133-145.

Yasar E., 2001. *Failure and failure theories for anisotropic rocks. In: Proceedings of the 17th International Mining Congress and Exhibition of Turkey IMCET*. Ankara: Chamber of Mining Engineers of Turkey.

Zhang X.M., Feng Y., Yang J.S., 2010. *Experimental study on anisotropic strength properties of sandstone*. Electronic Journal of Geotechnical Engineering **15**, 1325-1335.

Zhang X.P., Wong L.N.Y., 2014. *Displacement field analysis for cracking processes in bonded-particle model*. Bulletin of Engineering Geology & the Environment **73** (1), 13-21.